metals

MDPI

Article

Detrimental Effects of β_o-Phase on Practical Properties of TiAl Alloys

Toshimitsu Tetsui [1,*] and Kazuhiro Mizuta [2]

[1] National Institute for Materials Science, Tsukuba 305-0047, Ibaraki, Japan
[2] AeroEdge Co., Ltd., Ashikaga 329-4213, Tochigi, Japan; kazuhiro.mizuta@aeroedge.co.jp
* Correspondence: tetsui.toshimitsu@nims.go.jp

Abstract: The TNM alloy, a β_o-phase-containing TiAl alloy, has been withdrawn from use as a last-stage turbine blade in commercial jet engines as it suffered frequent impact fractures in service, raising doubts regarding the necessity of the β_o-phase in practical TiAl alloys. Here, we evaluate the practical properties required for jet engine blades for various TiAl alloys and investigate the effects of the β_o-phase thereupon. First, we explore the influence of the β_o-phase content on the impact resistance and machinability for forged Ti–43.5Al–xCr and cast Ti–46.0Al–xCr alloys; the properties deteriorate significantly at increasing β_o-phase contents. Subsequently, two practical TiAl alloys—TNM alloy and TiAl4822—were prepared with and without the β_o-phase by varying the heat treatment temperature for the former and the Cr concentration for the latter. In addition to impact resistance and machinability, the creep strength is significantly reduced by the presence of the β_o-phase. Overall, these findings suggest that the β_o-phase is an undesirable phase in practical TiAl alloys, especially those used for jet engine blades, because, although the disordered β-phase is soft at high temperatures, it changes to significantly more brittle and harder β_o-phase after cooling.

Keywords: titanium aluminides; impact resistance; machinability; creep strength; jet engine blades

Citation: Tetsui, T.; Mizuta, K. Detrimental Effects of β_o-Phase on Practical Properties of TiAl Alloys. *Metals* **2024**, *14*, 908. https://doi.org/10.3390/met14080908

Academic Editor: Francesca Borgioli

Received: 15 July 2024
Revised: 2 August 2024
Accepted: 7 August 2024
Published: 9 August 2024

1. Introduction

Elements such as Nb, Cr, Mo, Mn, and W are the main additives in TiAl alloys and function as β-stabilizers. These additive elements are present in practical TiAl alloys that were developed early, such as TiAl4822 (Ti–48Al–2Nb–Cr (at. %; this unit is omitted hereafter) [1–3], 45, 47XD (Ti–45, 47Al–2Nb–2Mn–0.8vol% TiB_2) [4–6], and DAT-TA2 (Ti–46.5Al–3.2Nb–0.8Cr–0.7Si–0.1C) [7]. Notably, the β-phase content in these initial TiAl alloys is minimal because of the low added amount.

From a practical standpoint, the β-phase has been actively used for ~20 years to forge TiAl alloys, which was previously considered impossible. At high forging temperatures, the β-phase transforms into a disordered bcc phase that significantly improves deformability and enables forming by forging. By contrast, after cooling, it changes into the ordered β_o(B2)-phase of an intermetallic compound. Ti–42Al–5Mn [8–10], which is a representative alloy with high β/β_o-phase content, can be readily deformed by hot forging during which the heated material is removed from the furnace and pressed at a high speed in the air using a die at a relatively low temperature, enabling the production of large parts [11].

In contrast, the TNM alloy (Ti–43.5Al–4Nb–1Mo–0.1B) [12–14], which is a representative forged TiAl alloy with low β/β_o-phase content, is not conducive to high-speed deformation while cooling owing to its low β-phase levels. Therefore, hot forging cannot be readily used to manufacture products that require no defects; instead, these are manufactured by isothermal forging, in which a high-temperature die is used in a high-temperature chamber, with deformation conducted at an extremely low speed. The TNM alloy was once used in Pratt & Whitney's PW1100G commercial aircraft jet engine [15]; however, it was discontinued and replaced with a common heat-resistant alloy owing to frequent impact

fractures caused by collisions with flying debris inside the engine [16]. In contrast, other jet engines such as General Electric's (GE) GEnx [15] and CFM International's LEAP [17,18] use large amounts of TiAl4822 cast material with virtually no β_o-phase and do not experience impact fracture or other problems. This extreme difference is undoubtedly related to the fact that the PW1100G engine, which is of a geared turbofan variety, exhibits greater collision energy with debris owing to its faster rotational speed than that of regular turbofan engines such as LEAP. Nevertheless, this variation was naturally anticipated in the design process; in other words, the differences in the material properties between TNM alloy and TiAl4822 are potentially responsible for their extreme disparity in practical use. The most significant difference between the two is the presence or absence of the β_o-phase.

Therefore, the present study was aimed at evaluating the need for the β/β_o-phase from a practical viewpoint and clarifying whether the β/β_o-phase offers any value for TiAl alloys other than improving forgeability. The assumed product is the last-stage turbine blades of a jet engine. The critical strength properties for this product include creep strength and high-/low-cycle fatigue strength at elevated temperatures. Concerning high-cycle fatigue strength, Sallot et al. [19] have already reported that the β_o-phase preferentially oxidized during prior atmospheric heating reduces fatigue strength. In terms of low-cycle fatigue strength, Nakatani et al. [20] reported that the preferential oxidation of the β_o-phase during testing reduces fatigue strength.

In addition to these strength properties, two other attributes are essential for fabricating high-performance and reliable jet engine blades. The first characteristic, impact resistance, is vital because of the disastrous experience with the TNM alloy. In essence, high impact resistance is critical to ensure that TiAl blades are reliable during operation and not easily damaged by collisions with debris. The second aspect, machinability [21], is important to reduce manufacturing costs, given that TiAl blades for jet engines are currently manufactured from simply shaped ingots cast in permanent molds [22] or from investment cast blade materials with large amounts of excess wall [23]. Even forged materials (TNM alloy) that have been used in the past have used blade-like materials with large amounts of excess wall [24]. Therefore, they must be processed into thin product blades by high-volume machining, and excellent machinability is required to reduce costs.

Considering these aspects, at first, Ti–43.5Al–xCr ternary forged alloys and Ti–46.0Al–xCr ternary cast alloys with different β_o-phase contents were prepared in this study by changing the amount of Cr, and the effects of the β_o-phase on impact resistance and machinability were investigated. Subsequently, two practical TiAl alloys—TNM alloy and TiAl4822—with and without the β_o-phase were prepared by varying the heat treatment temperature for the former and the Cr concentration for the latter, and the effects of β_o-phase on creep strength were evaluated in addition to impact resistance and machinability. Finally, the obtained results were scrutinized to determine whether the β/β_o-phase in practical TiAl alloys, especially those used for jet engine blades, offers benefits other than improving forgeability.

2. Materials and Methods

2.1. Materials

Ti–Al–xCr ternary alloys with varying β_o-phase contents were prepared by altering the Cr concentration to 2.0, 2.5, 3.0, 3.5, and 4.0 in the 43.5Al forged alloys and 46.0Al cast alloys. Furthermore, modified TNM alloys with and without the β_o-phase were prepared by varying the post-forging heat treatment temperature with the nominal composition of the TNM alloy (Ti–43.5Al–4.0NB–1.0Mo–0.1B). For the modified TiAl4822 alloys, the nominal Al concentration is 48; however, the material commonly used today has a slightly reduced Al concentration. Therefore, samples of modified TiAl4822 with and without the β_o-phase were prepared by changing the content of Cr slightly (1.79, 1.91, and 2.14) in Ti–47Al–2.0Nb.

The raw materials—Ti sponge, Al pellets, Cr grains, Nb thin plates, and Mo and TiB_2 powders—were induction melted in a CaO crucible in an atmosphere that was replaced

by Ar after vacuuming. The weight of one batch was ~850 g. After all the raw materials were melted, the resulting molten metal was kept for 3 min with the melting power applied and then poured into a metal mold that was divided into two parts. For the Ti–43.5Al–xCr ternary forged alloys and modified TNM alloys, cylindrical ingots with approximate dimensions of ø55 × 90 mm were produced by casting the molten metal into a metal mold with a cylindrical cavity. For the Ti–46.0Al–xCr ternary cast alloys and modified TiAl4822 alloys, the molten metal was cast in the shape of a material with a flat-plate-type specimen collection section measuring 60 × 90 × 16 mm with a feeder head above it.

Melting in a CaO crucible cannot prevent the increase in oxygen concentration caused by oxygen contamination from the crucible [25]; therefore, the oxygen concentration will be higher than that of the existing TiAl alloy materials used for jet engine blades, which are typically melted in a water-cooled Cu crucible [22]. Therefore, in this study, 0.15 mass% Ca was added in the form of an Al–10mass% Ca alloy for deoxidization. The added Ca combines with oxygen in the molten metal to form CaO, which is released from the molten metal surface in the form of fumes during melting. Furthermore, excess Ca is discharged as Ca fumes. Consequently, the oxygen concentration of the TiAl alloy material after casting is less than 0.1 mass%, and the Ca concentration is less than 0.05 mass%. The details of this process will be provided in a separate report. As an example, the results of the chemical analysis of the modified TiAl4822 alloy produced in this study are shown in Table 1. The impurity levels are not significantly different from those of the TiAl4822 material melted in a water-cooled Cu crucible.

Table 1. Chemical analysis results of modified TiAl4822 alloy produced in this study.

Composition (Mass%)												
Ti	**Al**	**Nb**	**Cr**	**Cu**	**Fe**	**Ni**	**Si**	**C**	**O**	**N**	**H**	**Ca**
Bal.	32.6	4.62	2.64	<0.005	0.023	0.008	0.014	<0.005	0.07	<0.002	<0.002	0.044

Hot forging was used in this study instead of isothermal forging for cost reasons. To manufacture the Ti–43.5Al–xCr ternary forged alloys and modified TNM alloys, the cylindrical ingots were coated with ATP610 [26] (Advanced Technical Products Supply Co., Inc., West Chester, Ohio, USA) for lubrication and insulation during forging. Each ingot was held in a furnace heated to 1330 °C for ~1 h, removed from the furnace, and then pressed in the direction of the ingot height in a single forging operation using a 300-ton hydraulic press, forming a pancake with an approximate diameter and thickness of 130 mm and 16 mm, respectively. Cracking occurred at the periphery of the forged material in the Ti–43.5Al–xCr ternary forged alloys with low Cr concentrations and in the modified TNM alloys; however, this did not affect the subsequent evaluations as they were conducted using the interior parts.

For the Ti–43.5Al–xCr ternary forged alloys, a heat treatment protocol of 1280 °C/5 h/furnace cooling (FC) was applied. For the TNM alloy, two-stage heat treatment is typically performed after forging [12]: air cooling after high-temperature holding, followed by FC after low-temperature holding. In the present study, samples (TNM alloys of nominal composition) with and without the β_o-phase were prepared by changing the heat treatment temperature of the first stage, with values of 1177, 1207, and 1237 °C selected based on preliminary heat treatment tests. After forging, the TNM alloy pancakes were maintained at each of these temperatures for 3 h and then air-cooled. Subsequently, in the second stage, all pancakes were subjected to the standard 850 °C/6 h/FC protocol used for TNM alloy. For the Ti–46.0Al–xCr ternary cast alloys and modified TiAl4822 alloys, casting defects were eliminated by performing hot isostatic pressing (HIP) [27] using the 1200 °C/4 h/186 MPa protocol commonly employed for TiAl4822 cast materials.

2.2. Methods for Evaluating Various Properties

2.2.1. Impact Resistance

The Charpy impact test is the simplest and most realistic method for evaluating the impact resistance of industrial materials and can be easily conducted at high temperatures; therefore, it was used in the present study to determine impact resistance. After heat treatment and HIP, the forged and cast materials were machined on their front and back surfaces to achieve a uniform thickness of 10 mm. Subsequently, prismatic specimens with dimensions of approximately 10 × 10 × 55 mm were produced by further processing.

The impact resistance of TiAl alloys is significantly lower than that of normal metallic materials; therefore, unnotched specimens and a small 30J hammer were used to measure accurately the differences between the alloys. Room temperature (RT) and 700 °C, which is reportedly close to the maximum service temperature of TiAl alloys intended for jet engine blades, were selected as the test temperatures. For the 700 °C tests, an electric furnace was installed next to the testing machine. Each specimen was placed in the furnace at 700 °C for ~1 h, removed from the furnace, and then quickly placed in the Charpy impact testing device. Notably, the sample removed from the electric furnace was tested within 5–10 s. All the alloys were tested approximately 10 times at RT and 700 °C, and the impact resistance of each alloy was compared with the mean value of the absorbed energy. Moreover, the standard deviation was calculated.

2.2.2. Machinability

Materials with less tool damage allow faster machining speeds and therefore reduce costs. Therefore, the machinability of each alloy was evaluated based on the magnitude of the tool damage. The details of the cutting tests are provided elsewhere [28]. Briefly, square K10 carbide inserts were mounted on a seven-blade cutter (ø100 mm diameter between circumferentially mounted insert tips), and dry milling was performed using a face milling machine. Although the tool coating and lubrication conditions (dry, wet, etc.) have a significant effect on the machinability, the tests were aimed at comparing the relative machinability of the different alloys; therefore, uncoated carbide inserts were used under dry conditions.

The cutting tests were performed after the complete removal of the alteration layer on the surfaces of the forged and cast materials, which were formed by heat treatment and HIP. The milling conditions were constant with a cutter rotation speed of 130 revolutions per minute (peripheral speed of the insert tip of 0.680 m/s), feed rate of 4.97 mm/s, and cutting depth of 0.2 mm per cut. This was repeated until approximately 100 g of sample volume was removed.

Wear-induced tool weight loss was evaluated by measuring the change in weight for the sum of seven inserts before and after the cutting tests using a high-resolution analytical balance with a minimum measurement value of 0.00001 g. The obtained tool weight loss was normalized by the weight of the sample removed to compare the relative effect of each alloy on tool damage (that is, the machinability of each alloy).

2.2.3. Other Properties

The microstructure of each alloy was examined using backscattered electron images acquired in compositional mode. In addition, the area ratio of each phase was determined by analyzing these images with image-processing tools. To this end, a section corresponding to the center of the plate thickness of the forged and cast materials was cut and polished. For modified TNM and TiAl4822 alloys, creep tests were conducted at 750 °C/225 MPa using round bar specimens (diameter = 4.0 mm) with a 20.0 mm long gauge section, and the relationship between test duration and creep strain was measured. Additionally, certain alloys were subjected to Vickers hardness tests using a 294 N load. The five-point average was obtained, and brittleness was simply assessed by observing cracks formed near the indentation.

3. Results

3.1. Ti–Al–xCr Ternary Forged and Cast Alloys

In the five forged materials—that is, Ti–43.5Al–xCr, with x = 2.0, 2.5, 3.0, 3.5, and 4.0—the circumferential cracks decreased with increasing Cr content (Figure 1). This was due to the increase in the amount of the disordered β-phase with increasing Cr incorporation at heating temperature (1330 °C) before forging. Therefore, the beneficial effect of the disordered β-phase in improving forgeability was confirmed.

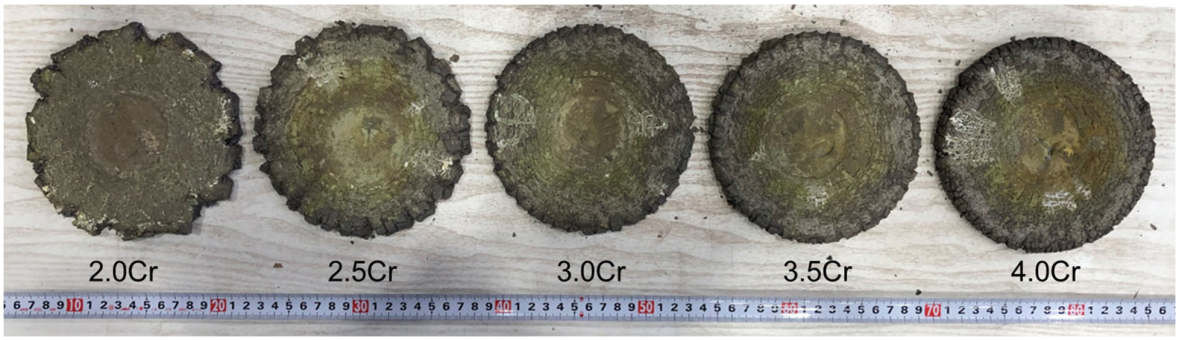

Figure 1. Appearance of Ti–43.5Al–xCr (at. %) alloys hot-forged after heating at 1330 °C.

The microstructures of the forged Ti–43.5Al–xCr alloys (x = 2.0, 2.5, 3.0, 3.5, and 4.0) were examined after the 1280 °C/5 h/FC heat-treatment protocol (Figure 2). Three phases were identified: the main phase is the γ-phase, the second phase is the α_2-phase, and the third phase is the β_o-phase. The alloys with 2.0Cr and 2.5Cr exhibited a fully lamellar structure and lacked the β_o-phase, whereas the remaining three alloys contained the β_o-phase, whose magnitude escalated with increasing Cr addition.

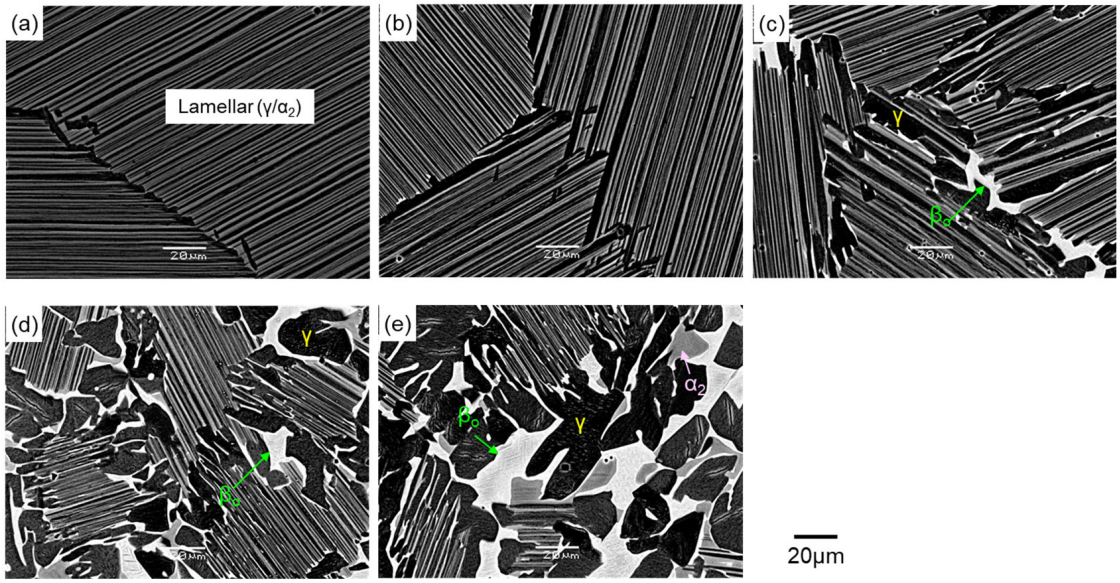

Figure 2. Backscattered electron images showing microstructures of forged Ti–43.5Al–xCr ternary alloys subjected to the 1280 °C/5 h/furnace cooling heat treatment protocol after hot-forged at 1330 °C: x = (**a**) 2.0Cr, (**b**) 2.5Cr, (**c**) 3.0Cr, (**d**) 3.5Cr, and (**e**) 4.0Cr.

The microstructures of the cast Ti–46.0Al–xCr alloys (x = 2.0, 2.5, 3.0, 3.5, and 4.0) subjected to the 1200 °C/4 h/186 MPa HIP treatment were subsequently analyzed (Figure 3). The same types of phases were present as in the forged alloys. The 2.0Cr-doped alloy exhibited a fully lamellar structure and contained a small amount of the α_2-phase but

lacked the β_o-phase. Contrarily, the remaining four alloys contained the β_o-phase, whose extent increased when the incorporated Cr increased.

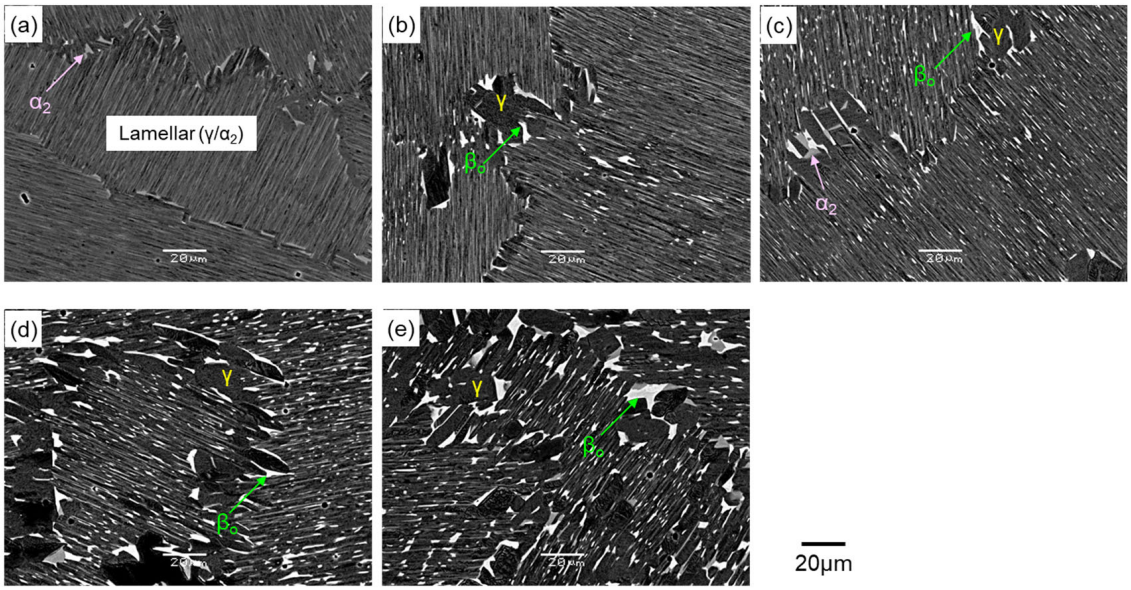

Figure 3. Backscattered electron images showing microstructures of cast Ti–46.0Al–xCr ternary alloys subjected to hot isostatic pressing (HIP) using the 1200 °C/4 h/186 MPa protocol: x = (**a**) 2.0Cr, (**b**) 2.5Cr, (**c**) 3.0Cr, (**d**) 3.5Cr, and (**e**) 4.0Cr.

The relationship between the area ratio of the α_2-phase (the second phase) and that of the β_o-phase (the third phase) vs. the Cr concentration—obtained by processing the backscattered electron images of the forged Ti-43.5Al-xCr and cast Ti-46.0Al-xCr alloys—is plotted in Figure 4. For both alloys, the area ratio of the α_2-phase decreases and that of the β_o-phase increases with increasing Cr concentration. The α_2-phase is mostly present in the lamellar structure, which indicates that the ratio of the lamellar structure decreases with increasing Cr concentration. A comparison of the forged and cast alloys reveals that the ratio of the β_o-phase in the former is higher due to the lower Al concentration.

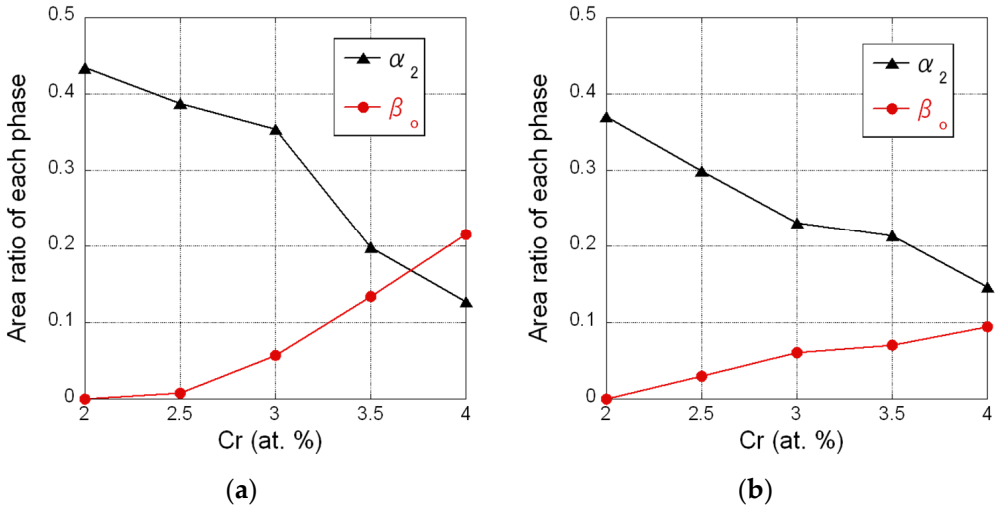

Figure 4. Relationship between Cr concentration and ratio of α_2- and β_o-phase in (**a**) forged Ti–43.5Al–xCr alloys and (**b**) cast Ti–46.0Al–xCr alloys.

The mean absorbed energy and the corresponding standard deviation were determined for the forged and cast Ti–Al–xCr ternary alloys from the Charpy impact tests

conducted at RT and 700 °C (Table 2). In addition, the relationship between the area ratio of the α_2-phase (the second phase) and that of the β_o-phase (the third phase) and the mean absorbed energy is shown in Figure 5. These results suggest that the factors responsible for the decrease in the mean absorbed energy at both RT and 700 °C in the forged and cast Ti–Al–xCr ternary alloys are the increase in the β_o-phase and the decrease in the α_2-phase (decrease in the lamellar structure ratio). The decrease in the impact resistance due to the decrease in the lamellar structure ratio was already confirmed in our previous study [21,28]. In addition to this, it is clear from this study that as the β_o-phase increases, the impact resistance decreases. Regarding the test temperatures used, the mean absorbed energy was higher at 700 °C than at RT for both the forged and cast alloys, possibly owing to the increased ductility while maintaining strength at 700 °C.

Table 2. Charpy impact test results at room temperature (RT) and 700 °C for forged Ti–43.5Al–xCr and cast Ti–46.0Al–xCr alloys.

Composition (at. %)		Production Method	Heat Treatment Protocol	Hot Isostatic Pressing (HIP) Conditions	Charpy Impact Test Results at RT		Charpy Impact Test Results at 700 °C	
Al	Cr				Mean Absorbed Energy (J/cm^2)	Standard Deviation (SD)	Mean Absorbed Energy (J/cm^2)	SD
43.5	2.0	Cast → hot-forging at 1330 °C	1280 °C/ 5 h/furnace cooling (FC)	-	5.85	0.57	10.16	2.22
	2.5				5.58	0.57	11.15	2.60
	3.0				5.04	0.56	11.13	1.88
	3.5				3.70	0.68	10.35	1.27
	4.0				3.47	0.29	7.71	1.06
46.0	2.0	Cast	-	1200 °C/ 4 h/ 186 MPa	5.22	0.61	11.37	1.57
	2.5				4.73	0.61	11.60	1.78
	3.0				4.57	0.75	11.46	2.24
	3.5				3.48	0.69	10.77	1.35
	4.0				3.25	0.48	9.22	1.38

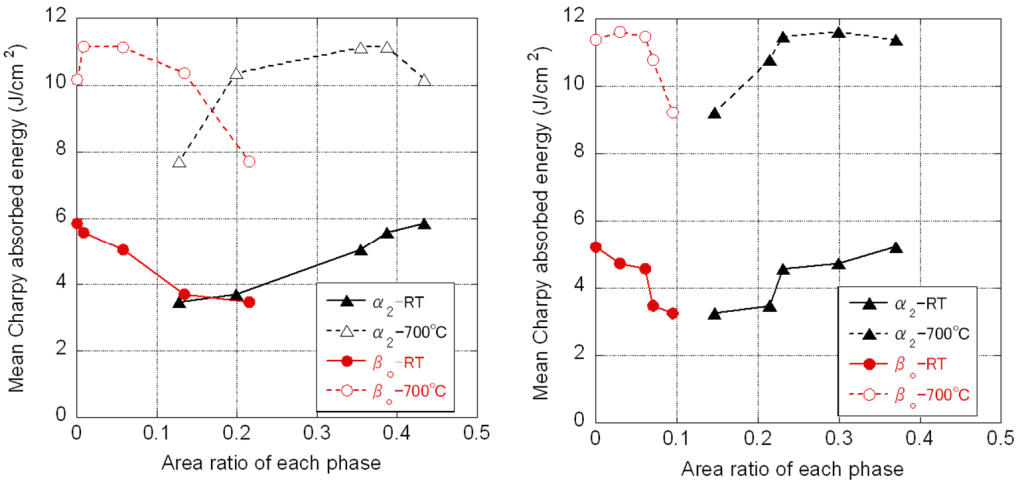

Figure 5. Relationship between the area ratio of α_2- and β_o-phase and the mean absorbed energy obtained in the Charpy impact test at RT and 700 °C for (**a**) forged Ti–43.5Al–xCr alloys and (**b**) cast Ti–46.0Al–xCr alloys.

The cutting test results of the forged and cast Ti–Al–xCr ternary alloys were analyzed to establish a relationship between tool weight loss and Cr concentration (Figure 6); the tool weight loss was normalized to the weight of the sample removed by cutting. The findings, in combination with the results shown in Figures 2–4, suggest that the extent of tool wear is independent of the α_2-phase (lamellar structure) ratio and increases with increasing β_o-phase content, confirming the negative effect of the β_o-phase on the machinability of the TiAl alloys.

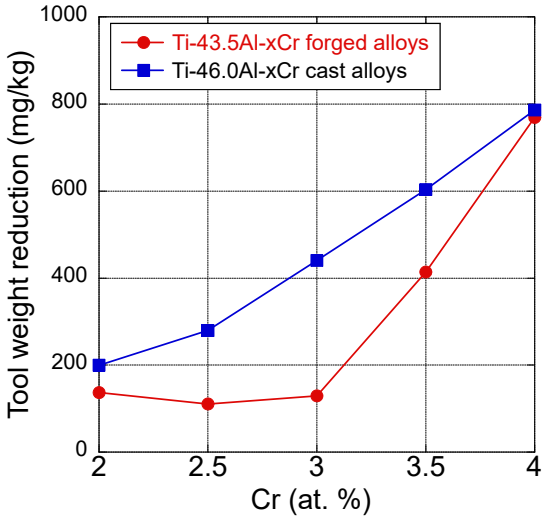

Figure 6. Results of machining tests conducted on forged Ti–43.5Al–xCr and cast Ti–46.0Al–xCr alloys, showing the relationship between Cr concentration and tool weight loss at each Cr incorporation stage.

3.2. Modified TNM and TiAl4822 Alloys

The microstructures of the modified TNM alloys in nominal composition were examined using different heat treatment temperatures in the first heat treatment stage after hot forging at 1330 °C (Figure 7). In the alloy heat treated at 1177 °C, the amount of the β_o-phase was high, whereas, in the alloy heat treated at 1207 °C, the microstructure was a mixture of lamellar structure and the α_2-, γ-, and β_o-phases, which resembles the previously reported standard microstructure of TNM alloy [12]. Moreover, in the alloy heat treated at 1237 °C, the β_o-phase almost disappeared and changed to a mixed microstructure containing a lamellar structure and the α_2- and γ-phases.

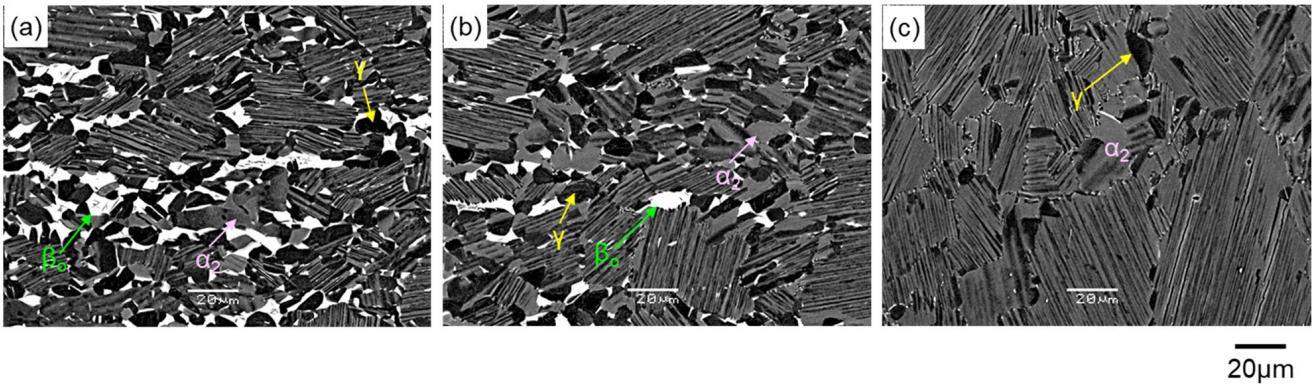

Figure 7. Backscattered electron images showing microstructures of modified TNM alloys hot-forged at 1330 °C and then subjected to the first heat treatment stage at (**a**) 1177, (**b**) 1207, and (**c**) 1237 °C for 3 h followed by air cooling and subjected to the second heat treatment stage at 850 °C for 6 h followed by furnace cooling.

The microstructures of modified TiAl4822 alloys (Ti–47Al–2.0Nb-xCr) with varying Cr contents (1.79, 1.91 and 2.14) were examined after subjecting them to HIP at 1200 °C/4 h/186 MPa (Figure 8). The 1.79Cr and 1.91Cr alloys exhibited a duplex structure with lamellar structure and γ-grains, in addition to a small amount of the α_2-grains. The 2.14Cr alloy exhibited a similar microstructure but with a β_o-phase.

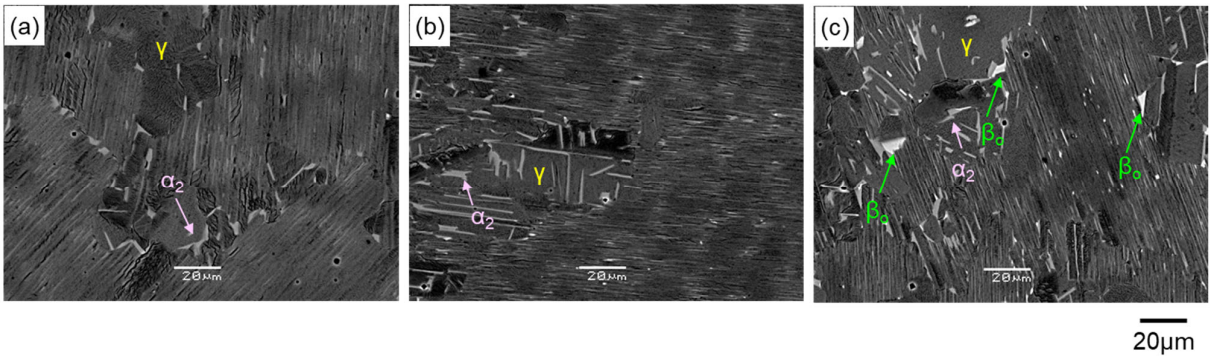

Figure 8. Backscattered electron images showing microstructures of modified TiAl4822 alloys after HIP at 1200 °C/4 h/186 MPa: (**a**) Ti–47.0Al–2.0Nb–1.79Cr, (**b**) Ti–47.0Al–2.0Nb–1.91Cr, and (**c**) Ti–47.0Al–2.0Nb–2.14Cr.

Subsequently, the average absorbed energy and standard deviation were determined for the modified TNM and TiAl4822 alloys from the Charpy impact tests conducted at RT and 700 °C (Table 3). Among the modified TNM alloys, the samples heat treated at 1177 and 1237 °C exhibited the lowest and highest absorbed energy, respectively, at both RT and 700 °C. In other words, the decrease in impact resistance with increasing β_o-phase content was estimated by a comparison of these findings with those shown in Figure 7. Among the modified TiAl4822 alloys, the absorbed energy of the alloy with 2.14Cr was the lowest both at RT and 700 °C, whereas that of the alloys with 1.79Cr and 1.91Cr did not differ significantly. These results, in combination with those shown in Figure 8, indicate that the impact resistance decreases when the β_o-phase is present.

Table 3. Charpy impact test results at RT and 700 °C for modified TNM and TiAl4822 alloys.

Alloys	Composition (at. %)					Production Method	Heat Treatment Protocol	HIP Conditions	Charpy Impact Test Results at RT		Charpy Impact Test Results at 700 °C	
	Al	Nb	Cr	Mo	B				Mean Absorbed Energy (J/cm^2)	SD	Mean Absorbed Energy (J/cm^2)	SD
TNM alloy	43.5	4.0	-	1.0	0.1	Cast → hot-forging at 1330 °C	1177 °C/3 h AC → 850 °C/6 h FC	-	5.86	1.41	6.07	0.91
							1207 °C/3 h AC → 850 °C/6 h FC		6.66	1.93	7.77	0.78
							1237 °C/3 h AC → 850 °C/6 h FC		8.43	2.21	8.50	1.30
TiAl 4822	47.0	2.0	1.79	-	-	Casting	-	1200 °C/ 4 h/186 MPa	6.08	1.08	15.54	3.12
			1.91						6.06	1.32	15.30	3.32
			2.14						4.59	0.98	12.34	2.05

Regarding the test temperatures, the increase in the absorbed energy of the modified TNM alloys at 700 °C was smaller than that at RT. Conversely, this increase was considerably greater for the modified TiAl4822 alloys presumably because the amount of the γ-phase in the TiAl4822 alloys was significantly higher than in the TNM alloys, resulting in improved ductility with maintained strength at 700 °C. However, the relationship of the heat treatment temperature for the modified TNM alloys or the amount of Cr added in the modified TiAl4822 alloys with the superiority in terms of impact resistance was the same as that at RT. Thus, the β_o-phase continued to exert a detrimental effect on the impact resistance of practical TiAl alloys at the operating temperature of jet engine blades.

The results of the cutting tests performed on the modified TNM and TiAl4822 alloys were subsequently analyzed (Figure 9). For the modified TNM alloys, the tool weight loss (normalized to the weight of the sample removed) was plotted against the first-stage heat treatment temperature. The results, in combination with those shown in Figure 7, indicate that the tool wear magnitude increases at increasing amounts of the β_o-phase, confirming the undesirable influence of the β_o-phase on the machinability of the modified TNM alloys.

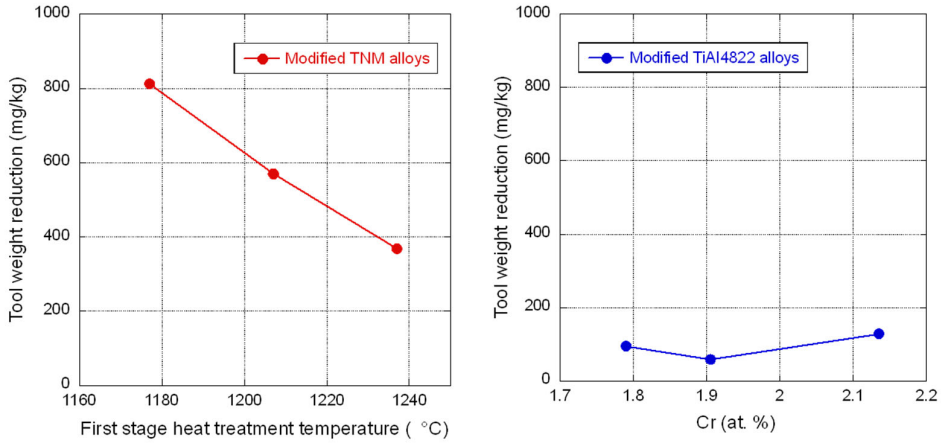

(**a**) (**b**)

Figure 9. Results of machining tests conducted on the modified TNM and TiAl4822 alloys, showing the relationship between the (**a**) first-stage heat treatment temperature and tool weight loss for modified TNM alloys, and (**b**) Cr content and tool weight loss for modified TiAl4822 alloys.

For the modified TiAl4822 alloys, the relationship between the Cr concentration and the scale of the tool weight loss was investigated. The tool wear of the modified TiAl4822 alloys was significantly lower than that of the modified TNM alloys. This was probably due to the presence of significantly higher and lower proportions of the softer γ-phase and the harder α_2-phase, respectively, in the modified TiAl4822 alloys than those in the modified TNM alloys. Among the modified TiAl4822 alloys, the tool wear of the 2.14Cr alloy was slightly higher than that of the 1.79Cr and 1.91Cr alloys. Essentially, these results, in combination with those shown in Figure 8, imply that the machinability decreases in the presence of the β_o-phase.

The relationship between test duration and creep strain was examined by subjecting the modified TNM and TiAl4822 alloys to creep tests at 750 °C/225 MPa (Figure 10). Among the modified TNM alloys, the alloys heat treated at 1177 and 1237 °C exhibited the lowest and highest creep strengths, respectively. These results demonstrate that the creep strength decreased significantly at increasing β_o-phase content. Among the modified TiAl4822 alloys, the alloy with 2.14Cr exhibited a lower creep strength than those of the alloys with 1.79 and 1.91Cr. Based on this result, we could conclude that a reduction in creep strength was observed owing to the presence of the β_o-phase.

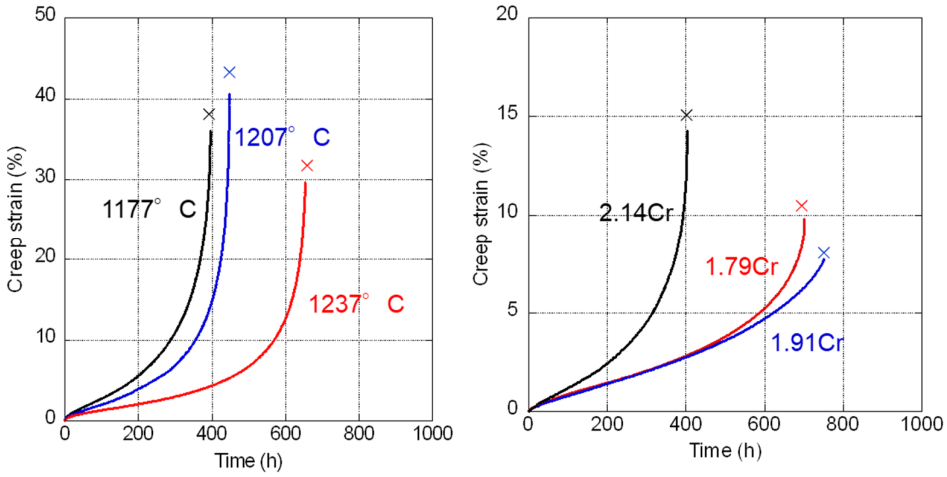

(**a**) (**b**)

Figure 10. Creep curves of (**a**) modified TNM alloys and (**b**) modified TiAl4822 alloys subjected to a creep test performed at 750 °C/225 MPa.

The microstructures near the ruptured positions in the creep test specimens were examined for the modified TNM alloy heat treated at 1177 °C (which exhibited the lowest creep strength among the modified TNM alloys), and the modified TiAl4822 alloy integrated with 2.14Cr (which showed the lowest creep strength among the modified TiAl4822 alloys) (Figure 11). The results reveal creep voids concentrated in the β_o-phase in both alloys. In other words, the microstructural analysis indicated that the creep strength of the β_o-phase was lower than that of the lamellar structure, γ-phase, and α_2-phase. Overall, these findings indicate that the β_o-phase adversely affected the creep strength of practical TiAl alloys, in addition to impact resistance and machinability. Notably, as mentioned earlier, the preferentially oxidized β_o-phase degrades high- and low-cycle fatigue properties at high temperatures [19,20]. In other words, the β_o-phase can have a significant detrimental effect on the strength properties that are critical for jet engine blades.

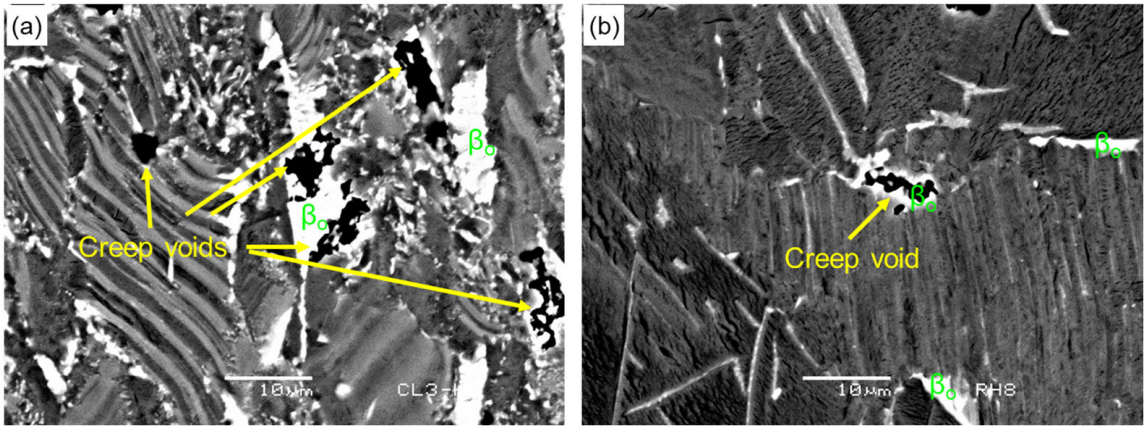

Figure 11. Microstructures near ruptured position in creep specimens, showing the locations of creep voids: (**a**) modified TNM alloy subjected to the first-stage heat treatment at 1177 °C and (**b**) modified TiAl4822 alloy with 2.14Cr.

4. Discussion

4.1. Summary of the Influence of Each Phase on the Practical Properties of TiAl Alloys

The basic phase of TiAl alloys is the γ-phase (TiAl phase). In practical TiAl alloys, the second phase, i.e., the α_2-phase, is formed by reducing the Al concentration. Because most of the α_2-phase exists in the form of a lamellar structure, the ratio of the α_2-phase is proportional to that of the lamellar structure. On the other hand, the third phase, i.e., the β/β_o-phase, is formed by adding more than a certain amount of β-stabilizing elements such as Cr and Mn, which are commonly added to practical TiAl alloys. Other factors affecting the properties of TiAl alloys include finer grain size and finer lamellar spacing. However, with regard to the former, it is difficult to obtain fine grains, especially in practical TiAl alloys for jet engine blades, because they must be heat treated or HIPed at high temperatures for long periods to ensure microstructural stability in service. On the other hand, the latter requires rapid cooling after high-temperature heat treatment, which requires special processes such as gas-fan cooling, resulting in higher costs. Therefore, the ratio of the α_2-phase (lamellar structure) and that of the β/β_o-phase is considered to have the greatest influence on the properties of practical TiAl alloys.

Based on the results obtained in this study and related references, we summarized the effects of the α_2- and β_o-phases ratios on each practical property in Table 4. These results indicate that the α_2-phase (lamellar structure) often has a positive effect, whereas the β_o-phase has only a negative effect.

Table 4. Summary of the effects of the α_2- and β_o-phases ratios on the practical properties of TiAl alloys.

Change in Phase Ratio	Impact Resistance RT	Impact Resistance 700 °C	Machinability	Creep Strength	High-Temperature Fatigue Strength
Increase in α_2-phase (increase in lamellar structure)	Improved	Improved	Small effect	Improved [29]	Varies depending on conditions [30]
Increase in β_o-phase	Reduced	Reduced	Reduced	Reduced	Reduced [19,20]

4.2. Causes of Negative Effects of β_o-Phase on Impact Resistance and Machinability

The reasons underlying the undesirable effects of the β_o-phase on impact resistance and machinability were then investigated using a simple method. Essentially, in the Ti–Al–Cr ternary system, single-phase alloys were prepared based on the phase diagram at 1200 °C [31,32] and evaluated. Alloys with compositions of Ti–40.5Al–10.0Cr, Ti–41.0Al–1.0Cr, and Ti–50.0Al–2.0Cr, which were designed to contain only the β_o-, α_2-, and γ-phases, respectively, were prepared. The melting method was identical to that described above, and microstructural observations and Vickers hardness tests at 294 N were performed on the cast materials at RT after heat treatment; these involved maintaining the samples at 1200 °C for 10 h followed by water quenching.

The microstructures, cracks formed near the indentation caused during the Vickers hardness test, and Vickers hardness values at RT were investigated for these alloys (Figure 12). A small amount of the γ-phase coexisted in the alloy designed to exhibit a single β_o-phase; however, the β_o-phase was predominant. The Vickers hardness of this alloy (HV 493) indicated that it was extremely hard. Moreover, the observed cracking around the indentation implied that this alloy was remarkably brittle. The alloy designed to exhibit a single α_2-phase contained a single α_2-phase; its hardness (HV 369) was lower than that of the aforementioned alloy with an almost single β_o-phase, and its cracking behavior was minor. The alloy intended to exhibit a single γ-phase also contained a single γ-phase; it exhibited the lowest hardness value (HV 200) among these alloys and showed only microscopic cracks around the indentation. These results indicate that although the disordered β phase is softer at high temperatures (forging temperature), it transforms into the β_o-phase, which is significantly more brittle and harder than the α_2- and γ- phases after cooling.

In the preceding discussion on impact resistance, the impact resistance of forged and cast Ti–Al–xCr ternary alloys, as well that of the practical TiAl alloys (modified TNM and TiAl4822 alloys), decreased at increasing β_o-phase content, presumably owing to the brittleness of the β_o-phase, as corroborated above. Furthermore, the machinability deteriorated at increasing β_o-phase content for different alloys; this was also related to the fact that the β_o-phase was significantly harder than the other phases, as verified above.

The α_2-phase is less brittle and less hard than the β_o-phase but more brittle and harder than the γ-phase; thus, it may cause negative effects similar to those of the β_o-phase. Nonetheless, because the α_2-phase is essentially present in TiAl alloys as a phase that forms lamellar structures, and a softer γ-phase exists between the thin α_2-phase plates, the combined effect of the microstructure seemingly mitigates the brittleness and hardness of the α_2-phase to a certain extent. However, unlike the α_2-phase, the β_o-phase cannot co-exist as a composite structure with the γ-phase but exists independently, suggesting that its brittleness and hardness cannot be mitigated by the microstructural factors.

Composition (at. %)	Targeted phase	Microstructure	Cracks near indentation	Vickers hardness (294N)	
				Average of 5 points (HV)	SD
Ti-40.5Al-10.0Cr	β_o	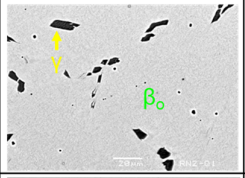	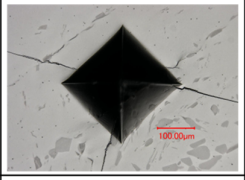	493	3.8
Ti-41.0Al-1.0Cr	α_2	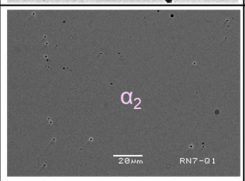	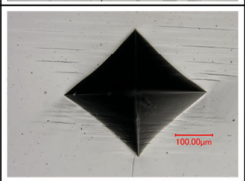	369	5.3
Ti-50.0Al-2.0Cr	γ	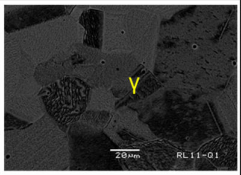	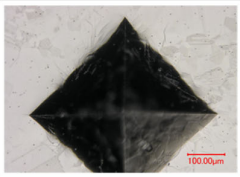	200	2.4

20μm

Figure 12. Results obtained from tests conducted to analyze the microstructure, Vickers hardness (HV), and brittleness at room temperature for alloys aimed at a single phase corresponding to each phase in the Ti–Al–Cr ternary alloy system at 1200 °C.

4.3. Assessment of Various Existing TiAl Alloys Assuming the Harmfulness of β_o-Phase

4.3.1. Cast TiAl Alloys

For cast TiAl alloys, there is no need for the disordered β-phase that is required for the forging process; therefore, the composition should be designed to prevent the formation of the detrimental β_o-phase. Among the known TiAl cast alloys, TiAl4822 (Ti–48Al–2Nb–2Cr) [1–3]—which is practically used to fabricate jet engine blades—contains 2% Nb and 2% Cr, which exhibit small and large β-stabilizing effects, respectively. As confirmed in the present study, a slight increase in Cr concentration will lead to the formation of the harmful β_o-phase. However, this rarely occurs with the current compositional specification ranges; therefore, this is not considered a major problem. Furthermore, it would be perfectly fine to limit the Cr content a little lower than the current specification. The 45, 47XD alloy (Ti–45, 47Al–2Nb–2Mn–0.8vol% TiB_2) [4–6], which had been considered for fabricating jet engine blades for Rolls-Royce [33], is perfectly safe because it contains 2% Nb and 2% Mn, which has a lesser β-stabilizing effect than that of Cr. Additionally, DAT-TA2 (Ti–46.5Al–3.2Nb–0.8Cr–0.7Si–0.1C) [7]—which is being used to fabricate turbine wheels for passenger car turbochargers—has a slightly increased Nb content than that in the two aforementioned practical alloys; notably, this is perfectly acceptable given the low Cr content. In essence, the TiAl cast alloys developed and used in the distant past are excellent in that the addition of a small amount of β-stabilizing elements improves their properties and suppresses the formation of the harmful β_o-phase.

In contrast, modern TiAl alloys such as TNB-V2 (Ti-45Al-8Nb-0.2C) [34] and IRIS (Ti-48Al-2W-0.08B) [35] contain many β-stabilizing elements. Only Nb, which has a small β-stabilizing effect, is added in the former; however, the amount incorporated is sufficiently large for forming the β_o-phase. Meanwhile, 2% W—which has an extremely large β-stabilizing effect—is added to the latter, resulting in an abundant β_o-phase content. Newer TiAl alloys, including these alloys, contain large amounts of additives mainly to improve strength and oxidation resistance; however, the practical properties required for jet engine blades, such as impact resistance and machinability, are considered to be significantly inferior to those of the practical TiAl alloys developed earlier owing to the presence of

the β_o-phase. These observations underscore the superiority of the previously developed TiAl alloys.

Regarding the additive elements, Nb was added mainly to improve the oxidation resistance of TiAl alloys; however, no significant differences in oxidation resistance have been observed between TiAl alloys in which 5% and 10% Nb were incorporated [36]. Therefore, large amounts of Nb need not be added; this can prevent β_o-phase formation and reduce material costs. Additionally, W and Mo exhibit a large β-stabilizing effect; therefore, even small levels of incorporation will produce the β_o-phase. Similar to Nb, W was added to improve oxidation resistance [37,38]; however, because W induces the same improvement in oxidation resistance as that of Nb but at considerably lower levels, it could act as a beneficial additive when incorporated within the range where no β_o-phase is produced. Furthermore, Mo does not need to be incorporated into cast alloys as it does not provide any property-enhancing benefits other than disordered β-phase stabilization for improved forgeability. Additionally, Cr and Mn act as beneficial additives, improving properties such as ductility and impact resistance [39] when added in the range in which the β_o-phase does not form.

4.3.2. Forged TiAl Alloys

As confirmed for the forged Ti–43.5Al–xCr ternary alloys in this study, the β_o-phase could be eliminated by heat treatment when the Cr levels incorporated in them were $\leq$2.5%; but the forgeability was significantly reduced (Figure 1). At Cr levels of $\geq$3.0 at. %, which led to moderate forgeability, the β_o-phase remained after the heat treatment. From these results, it can be said that the impact resistance, machinability, and creep strength of the forged TiAl alloys with a certain degree of forgeability were inevitably inferior to those of the cast TiAl alloys without the β_o-phase. These findings reveal that the application of forged TiAl alloys is limited to large parts that cannot be produced using current TiAl alloy casting technologies. However, in such cases, the deterioration of various properties is inevitable.

Conversely, the TNM alloy is very interesting. In the present study, the β_o-phase was almost eliminated by heat treatment at 1237 °C in the modified TNM alloys with nominal composition. The melting and forging methods used in this study are different from those used for the TNM alloy used in jet engine blades, and thus do not faithfully reproduce the material in practical use. Contradictorily, several cases have been reported where the β_o-phase of TNM alloy has been eliminated by heat treatments [40–42]. Therefore, it is believed that the β_o-phase could be almost eliminated in the TNM alloy used in actual jet engine blades. In such cases, the impact resistance, machinability, and creep strength can be significantly improved, as shown in this study. In addition, fatigue strength, which has been reduced by preferential oxidation of the β_o-phase [19,20], should also be improved. It is very interesting why the β_o-phase was not removed in the TNM alloy commercialized for jet engine blades.

5. Conclusions

In this study, the influence of the β_o-phase on the practical properties of TiAl alloys was investigated for the use case of a last-stage turbine blade in a jet engine using 43.5Al forged alloys and 46.0Al cast alloys in a Ti–Al–xCr ternary system and two practical TiAl alloys (TNM alloy and TiAl4822). The salient results are outlined below:

- For the forged and cast Ti–Al–xCr ternary alloys, the impact resistance at RT and 700 °C, as well as the machinability, decreased significantly as the β_o-phase content increased.
- The results of modified TNM and TiAl4822 alloys show that the β_o-phase, present within the material, reduced the creep strength, impact resistance, and machinability.
- Although the disordered β-phase is soft at high temperatures (forging temperature), it changes to the ordered β_o-phase, which is significantly more brittle and harder after

cooling. Thus, the detrimental effect of the β_o-phase on the impact resistance and machinability can be attributed to this change.
- An evaluation of various existing TiAl alloys developed to date with respect to the presence or absence of the β_o-phase suggests that the practical properties of β_o-phase-free TiAl alloys (that were developed in the distant past) are superior to those of more recent TiAl alloys that contain the β_o-phase.
- Finally, it can be concluded that the β_o-phase should not be included in practical TiAl alloys, especially those used for jet engine blades.

Author Contributions: Conceptualization, T.T. and K.M.; methodology, T.T.; software, T.T.; validation, T.T.; formal analysis, T.T.; investigation, T.T.; resources, T.T. and K.M.; data curation, T.T.; writing—original draft preparation, T.T.; writing—review and editing, K.M.; visualization, T.T.; supervision, T.T.; project administration, K.M.; funding acquisition, K.M. All authors have read and agreed to the published version of the manuscript.

Funding: This research was funded by the Japan Science and Technology Agency, grant number AS0216001.

Data Availability Statement: Data will be made available on request.

Conflicts of Interest: The authors declare no conflicts of interest.

References

1. Bartolotta, P.; Barrett, J.; Kelly, T.; Smashey, R. The use of cast Ti-48Al-2Cr-2Nb in jet engines. *JOM* **1997**, *49*, 48–50. [CrossRef]
2. Xu, R.; Li, M.; Zhao, Y. A review of microstructure control and mechanical performance optimization of γ-TiAl alloys. *J. Alloys Compd.* **2023**, *932*, 167611. [CrossRef]
3. Feng, J.; Gui, W.; Liu, Q.; Bi, W.; Ren, X.; Liang, Y.; Lin, J.; Luan, B. Ti-48Al-2Cr-2Nb alloys prepared by electron beam selective melting additive manufacturing: Microstructural and tensile properties. *J. Mat. Res. Technol.* **2023**, *26*, 9357–9369. [CrossRef]
4. Larsen, D.E.; Christodoulou, L.; Kampe, S.L.; Sadler, R. Investment-cast processing of XD™ near-γ titanium aluminides. *Mater. Sci. Eng. A* **1991**, *144*, 45–49. [CrossRef]
5. McQuay, P.A.; Simpkins, R.; Seo, D.Y.; Bieler, T.R. Alloy and process improvements for cast gamma TiAl alloy applications. In *Gamma Titanium Aluminides*; Kim, Y.W., Dimiduk, D.M., Loretto, M.H., Eds.; The Minerals, Metals & Materials Society: Warrendale, PA, USA, 1999; pp. 197–207.
6. Shagñay, S.; Cornide, J.; Ruiz-Navas, E.M. Sliding wear behavior of intermetallic Ti-45Al-2Nb-2Mn-(at. %)-0.8vol%TiB2 processed by centrifugal casting and hot isostatic pressure: Influence of microstructure. *Materials* **2022**, *15*, 8052. [CrossRef] [PubMed]
7. Koyanagi, Y.; Sumi, Y.; Takabayashi, H. Development of titanium aluminide alloy with good high temperature properties for turbine wheel. *Denki Seiko* **2014**, *15*, 121–125. (In Japanese)
8. Xu, H.; Li, X.; Xing, W.; Shu, L.; Ma, Y.; Liu, K. Processing map and hot working mechanism of as-cast Ti-42Al-5Mn alloy. *Adv. Eng. Mater.* **2018**, *20*, 1701059. [CrossRef]
9. Li, X.; Tang, H.; Xing, W.; Zhao, P.; Chen, B.; Ma, Y.; Liu, K. Microstructural stability, phase evolution and mechanical properties of a forged W-modified high-Mn β-γ-TiAl alloy. *Intermetallics* **2021**, *136*, 107230. [CrossRef]
10. Graf, G.; Seyffertitz, M.; Spoerk-Erdely, P.; Clemens, H.; Stark, A.; Hatzenbichler, L.; Holec, D.; Burtscher, M.; Kiener, L.; Li, X.; et al. On the stability of Ti(Mn, Al)$_2$ C14 Laves phase in an intermetallic Ti-42Al-5Mn alloy. *Intermetallics* **2023**, *161*, 107962. [CrossRef]
11. Tetsui, T. Practical use of hot-forged-type Ti-42Al-5Mn and various recent improvements. *Metals* **2021**, *11*, 1361. [CrossRef]
12. Clemens, H.; Mayer, S. Design, processing, microstructure, properties, and applications of advanced intermetallic TiAl alloys. *Adv. Eng. Mater.* **2013**, *15*, 191–215. [CrossRef]
13. Kastenhuber, M.; Klein, T.; Clemens, H.; Mayer, S. Tailoring microstructure and chemical composition of advanced γ-TiAl based alloys for improved creep resistance. *Intermetallics* **2018**, *97*, 27–33. [CrossRef]
14. Yang, G.; Xu, X.; Hao, G.; Zhai, Y.; Wang, H.; Liang, Y.; Lin, J. Microstructure evolution, deformation behavior and processing performance of TNM TiAl alloy. *J. Mater. Sci.* **2023**, *58*, 5530–5551. [CrossRef]
15. Bewlay, B.P.; Nag, S.; Suzuki, A.; Weimer, M.J. TiAl alloys in commercial aircraft engines. *Mater. High Temp.* **2016**, *33*, 549–559. [CrossRef]
16. Hemmerdinger, J. FlightGlobal.com, FAA Orders PW1100G Low-Pressure Turbine Blade Replacement. 2019. Available online: https://www.flightglobal.com/engines/faa-orders-pw1100g-low-pressure-turbine-bladereplacement/135575.article (accessed on 24 May 2024).
17. Perrut, M.; Caron, P.; Thomas, M.; Couret, A. High temperature materials for aerospace applications: Ni-based superalloys and γ-TiAl alloys. *C.R. Phys.* **2018**, *19*, 657–671. [CrossRef]

18. Williams, J.C.; Boyer, R.R. Opportunities and issues in the application of titanium alloys for aerospace components. *Metals* **2020**, *10*, 705. [CrossRef]
19. Sallot, P.; Monchoux, J.P.; Joulie, S.; Couret, A.; Thomas, M. Impact of β-phase in TiAl alloys on mechanical properties after high temperature air exposure. *Intermetallics* **2020**, *119*, 106729. [CrossRef]
20. Nakatani, M.; Shimono, A.; Yamamoto, T.; Hiyoshi, N.; Itoh, T. Low cycle fatigue properties in forged TiAl alloy Ti-43Al-5V-4Nb with triplex microstructure. *J. Soc. Mat. Sci. Jpn.* **2021**, *70*, 111–117. (In Japanese) [CrossRef]
21. Tetsui, T. Identifying low-cost, machinable, impact-resistant TiAl alloys suitable for last-stage turbine blades of jet engines. *Intermetallics* **2024**, *168*, 108263. [CrossRef]
22. Güther, V.; Allen, M.; Klose, J.; Clemens, H. Metallurgical processing of titanium aluminides on industrial scale. *Intermetallics* **2018**, *103*, 12–22. [CrossRef]
23. Brotzu, A.; Felli, F.; Mondal, A.; Pilone, D. Production issues in the manufacturing of TiAl turbine blades by investment casting. *Procedia Struct. Integr.* **2020**, *25*, 79–87. [CrossRef]
24. Janschek, P. Wrought TiAl blades. *Mater. Today Proc.* **2015**, *2*, S92–S97. [CrossRef]
25. Gomes, F.; Barbosa, J.; Silva Ribeiro, C. Induction melting of γ-TiAl in CaO crucibles. *Intermetallics* **2008**, *16*, 1292–1297. [CrossRef]
26. ATP® 610, Advanced Technical Products Supply Co., Inc. Available online: https://www.knowde.com/stores/advanced-technical-products-supply/products/atp-610 (accessed on 13 May 2024).
27. Mizuta, K.; Hijikata, Y.; Fujii, T.; Gokan, K.; Kakehi, K. Characterization of Ti-48Al-2Cr-2Nb built by selective laser melting. *Scr. Mater.* **2021**, *203*, 114107. [CrossRef]
28. Tetsui, T. Effect of microstructure on impact resistance and machinability of TiAl alloys for jet engine turbine blade applications. *Metals* **2023**, *13*, 1235. [CrossRef]
29. Morris, M.A.; Lipe, T. ICreep deformation of duplex and lamellar TiAl alloys. *Intermetallics* **1997**, *5*, 329–337. [CrossRef]
30. Kumpfert, J.; Kim, Y.W.; Dimiduk, D.M. Effect of microstructure on fatigue and tensile properties of the gamma TiAl alloy Ti-46.5Al-3.0Nb-2.1Cr-0.2W. *Mater. Sci. Eng.* **1995**, *A192/193*, 465–473. [CrossRef]
31. Kriegel, M.J.; Pavlyuchkov, D.; Cupid, D.M.; Fabrichnaya, O.; Heger, D.; Rafaja, D.; Seifert, H.J. Phase equilibria at 1473 K in the ternary Al–Cr–Ti system. *J. Alloys Compd.* **2013**, *550*, 519–525. [CrossRef]
32. Shaaban, A.; Wakabayashi, H.; Nakashima, H.; Takeyama, M. Phase equilibria among β/α/α2/γ phases and phase transformations in Ti-Al-Cr system at elevated temperatures. *MRS Adv.* **2019**, *4*, 1471–1476. [CrossRef]
33. Voice, W. The future use of gamma titanium aluminides by Rolls-Royce. *Aircr. Eng. Aerosp. Technol.* **1999**, *71*, 337–340. [CrossRef]
34. Appel, F.; Paul, J.D.H.; Oehring, M.; Buque, C.; Klinkenberg, C.; Cameiro, T. Recent developments of TiAl alloys towards improved high-temperature capability. In *Niobium for High-Temperature Applications*; Kim, Y.W., Carneiro, T., Eds.; TMS: Pittsburgh, PA, USA, 2004; pp. 139–152.
35. Couret, A.; Reyes, D.; Thomas, M.; Ratel-Ramond, N.; Deshayes, C.; Monchoux, J.-P. Effect of ageing on the properties of the W-containing IRIS-TiAl alloy. *Acta Mater.* **2020**, *199*, 169–180. [CrossRef]
36. Yoshihara, M.; Miura, K. Effects of Nb addition on oxidation behavior of TiAl. *Intermetallics* **1995**, *3*, 357–363. [CrossRef]
37. Donchev, A.; Mengis, L.; Couret, A.; Mayer, S.; Clemens, H.; Galetz, M. Effects of tungsten alloying and fluorination on the oxidation behavior of intermetallic titanium aluminides for aerospace applications. *Intermetallics* **2021**, *139*, 107270. [CrossRef]
38. Zhao, P.; Li, X.; Tang, H.; Ma, Y.; Chen, B.; Xing, W.; Liu, K.; Yu, J. Improved high temperature oxidation properties for Mn-containing beta-gamma TiAl with W addition. *Oxid. Met.* **2020**, *93*, 433–448. [CrossRef]
39. Tetsui, T. Selection of additive elements focusing on impact resistance in practical TiAl cast alloy. *Metals* **2022**, *12*, 544. [CrossRef]
40. Hilleringmann, M.; Schievenbusch, J.; Zapala, P.; Bünck, M. Microstructure and mechanical properties of TNM titanium aluminide alloy after heat treatment and different cooling conditions. In *Intermetallics 2021: Programme and Abstracts*; Educational Center: Kloster Banz, Germany, 2021; O-TA-14; pp. 86–87.
41. Schwaighofer, E.; Clemens, H.; Mayer, S.; Lindemann, J.; Klose, J.; Smarsly, W.; Güther, V. Microstructural design and mechanical properties of a cast and heat-treated intermetallic multi-phase g-TiAl based alloy. *Intermetallics* **2014**, *44*, 128–140. [CrossRef]
42. Rittinghaus, S.-K.; Hecht, U.; Werner, V.; Weisheit, A. Heat treatment of laser metal deposited TiAl TNM alloy. *Intermetallics* **2018**, *95*, 94–101. [CrossRef]